

Effect of the Cooling Rate on the Microstructure and Properties of C92900 Bronze

V. E. Bazhenov^{a, *}, A. Yu. Titov^a, I. V. Shkalei^b, A. V. Sannikov^a, A. A. Nikitina^a, I. V. Plisetskaya^a,
A. I. Bazlov^a, A. M. Mezrin^b, and A. V. Kolygin^a

^a National University of Science and Technology MISIS, Moscow, Russia

^b Ishlinsky Institute for Problems in Mechanics, Russian Academy of Sciences, Moscow, Russia

*e-mail: V.E.Bazhenov@gmail.com

Received August 23, 2020; revised November 12, 2020; accepted November 17, 2020

Abstract—In mechanical engineering, antifriction tin bronzes are used for manufacturing friction parts, for example, C92900 bronze, which is used on aircraft braking systems. One way to improve the properties of leaded tin bronzes is to increase the cooling rate during solidification. In this work, the effect of the cooling rate and the changes in the content of alloying elements within the limits established by industry standards on the properties of C92900 bronze are investigated. In order to provide different cooling rates, the alloys are casted into molds made of resin-bonded sand, steel, and graphite, for which the cooling rates were 0.4, 5, and 14.6°C/s. The influence of the cooling rate and the composition of bronze on the freezing range, macrostructure, microstructure, thermal conductivity, hardness, tensile properties, and wear rate are investigated. By means of differential thermal analysis, it is shown that upper limit alloying of C92900 bronze leads to a decrease in the solidus temperature by 40°C, which should be considered during deformation processing and heat treatment. An increase in the cooling rate during the solidification of C92900 bronze ingots provides a significant grain refinement and change in the amount, size, and morphology of the phases. For example, in the case of metallic and graphite mold casting, the size of the lead particles decreases and its circularity increases. The change in the Sn content within the range established by industrial standard has a significant effect on the intermetallic γ -(Cu, Ni)₃Sn phase fraction. The increase in the cooling rate has no significant effect on the thermal conductivity of C92900 bronze, but it leads to an increase in hardness by 30 HB. It also improves the yield strength and ultimate tensile strength of the bronze. The wear test, carried out in accordance with the shaft–partial insert scheme in a kerosene medium using a steel counterbody, shows that an increase in the cooling rate during solidification leads to an increase in the wear rate of bronze from $\sim 0.4 \times 10^{-8}$ to $\sim 1.2 \times 10^{-8}$. The change in the bronze composition within the industrial standard range has practically no effect on the wear rate, but leads to a slight increase in the coefficient of friction.

Keywords: antifriction bronze, C92900, cooling rate, wear rate, mechanical properties, microstructure

DOI: 10.3103/S1067821221030044

INTRODUCTION

Tin bronzes have high strength, corrosion, and antifriction properties [1, 2]. They are used in mechanical engineering in parts operating on friction at medium loads and sliding speeds. In particular, items made of C92900 bronze are used in the components of aircraft braking systems [3, 4]. The requirements for the mechanical properties of C92900 bronze are low: ultimate strength 250 MPa, elongation 5%, and hardness 75 HB [5].

In accordance with the literature data, the microstructure of C92900 bronze consists of a solid solution based on copper (Cu), a tin-rich intermetallic phase δ -Cu₃₁Sn₈, and a solid solution based on lead (Pb) [1–3, 6, 7]. The copper solid solution provides plas-

ticity and is the matrix for the rest of the structural components. The intermetallic compound with tin provides bearing capacity due to its coherence with the matrix and increases wear resistance due to its higher hardness; lead particles contribute to the formation of a solid lubricating film on friction surfaces and improve machinability [8–11]. Nickel in bronze helps reduce the rate of oxidation [12].

It is known that bronzes containing 10 wt % Sn have a wide freezing range and, at low cooling rates, a large proportion of shrinkage porosity is observed in the ingot structure [1, 5, 13]. The porosity can be reduced by decreasing the width of the two-phase region formed in the solidifying ingot, increasing the cooling rate, or providing directional solidification [5, 14–16].

Table 1. Composition of C92900 bronze

Alloy	Main components, wt %			
	Cu	Sn	Ni	Pb
<i>L</i> (at lower limit)	Bal.	8.99	2.85	2.29
<i>U</i> (at upper limit)	Bal.	11.23	3.99	3.41
C92900 (UNS)	Bal.	9–11	2.8–4	2.0–3.2

An increase in the cooling rate when casting tin–lead bronzes leads to an increase in strength, hardness, cyclic durability, and elongation at fracture [2, 6, 17–19]. A comparative study of the behavior of bronzes of various compositions showed that there is no direct relationship between mechanical properties and wear resistance [9].

The wear characteristics of bronze are determined to the greatest extent by the microstructure of the alloy [9]. An increase in the cooling rate during the production of parts from tin–lead bronzes leads to an increase in the volume fraction of the intermetallic phase in the structure and a decrease in the size of lead particles [3, 17, 20–23]. It was found that an increase in the cooling rate leads to an increase in wear [6, 17–19]. Thus, the authors of [19] argue that the formation of large aggregates of the intermetallic phase and (Pb) is necessary to ensure high wear resistance. However, there is another opinion about the effect of (Pb) based on the fact that the tribological properties are higher when the particles of the lubricating phase are small, since in this case a greater amount of them is formed, which leads to a more uniform formation of the lubricating film [24].

The aim of this work was to study the effect of the cooling rate and the content of alloying elements on the macrostructure, microstructure, mechanical, and tribological properties of C92900 bronze.

MATERIALS AND RESEARCH METHODS

Samples of C92900 bronze of two compositions were prepared: according to the lower (*L*) and upper (*U*) alloying limits in accordance with Unified Numbering System (UNS) for Copper and Copper Alloys. Copper (99.9% purity), tin (99.92%), lead (99.985%), and nickel (99.93%) were used as a charge. For the convenience of introducing nickel, a Cu–10 wt % Ni master alloy was prepared. The alloy and master alloy were melted in a high-frequency induction furnace in a clay-graphite crucible. When obtaining the master alloy after melting the copper, nickel was introduced at a temperature of 1250–1300°C. To melt the alloy, copper and a Cu–10 wt % Ni master alloy were charged into the crucible. To create a reducing atmosphere, a broken electrode graphite of the GE brand (TU 1915-086-00200851–2007) was applied to the surface of the melt. Tin was introduced at a temperature of ~1200°C.

Lead was added last, after which the melt was cast. The composition of the alloys, determined using a Bruker Q4 Tasman optical emission spectrometer (Germany), is shown in Table 1.

To ensure different cooling rates, the alloys were poured into resin-bonded sand (sand further), steel, and graphite molds. Sand molds were obtained using the alpha-set process. In this case, a resin of the brand FS-01 (TU 2221-010-38267160–2012) and an A-30 hardener (TU 2494-001-95197502–2006) (Intema grupp, Russia) were used. The steel mold was made of 1015 grade steel, and the graphite mold was made of low-ash graphite of the GMZ grade. The temperature of pouring the melt into the molds was 1100°C. Cylindrical ingots with a diameter of 60 and 35 mm, respectively, with the same height of 150 mm, were obtained in molds made of sand and steel and, in graphite, a rectangular ingot with a cross section of 20 × 120 mm and a height of 100 mm was obtained. To determine the cooling rate, K-type thermocouples were immersed in the melt when pouring started and their readings were recorded until the ingots were completely cooled using a BTM-4208SD thermometer (Lutron, Israel).

The microstructure of the alloys and the content of elements in the phases were investigated using a Vega SBH3 scanning electron microscope (SEM) (Tescan, Czech Republic) with an Oxford energy dispersive microanalysis attachment. The proportion of phases in the structure, as well as the sizes and shapes of the phases, were determined using the ImageJ 1.52a image analysis software (National Institutes of Health, United States) using parameters such as the Feret diameter and circularity (*C*). The Feret diameter is the maximum distance between two tangents to the contour of the measured object [25]. It is used when the measured objects (in this case, the phases in the microstructure of the alloy) have an irregular shape. Circularity allows you to estimate how close the analyzed objects are in shape to a circle and is calculated by the equation [25]

$$C = 4\pi S/P^2, \quad (1)$$

where *S* and *P* are the area and perimeter of the object.

It can be seen that, when substituting the equations for the area and perimeter of a circle in formula (1), the value *C* = 1; i.e., the closer the circularity value is to one, the closer the object is to the circle.

The macrostructure of the alloys was studied using an Axio Observer.D1m optical microscope (Carl Zeiss, Germany). The identification of grain boundaries was carried out using an etchant with a composition of 5 g FeCl₃ + 15 mL HCl + 50 mL H₂O. The grain size was determined by the linear intercept method using the Sizer program (Department of Physical Metallurgy of Non-Ferrous Metals, National University of Science and Technology MISIS).

The liquidus and solidus temperatures of the alloy were estimated using differential scanning calorimetry (DSC) on an SDT Q600 analyzer from TA Instruments (United States). The tests were carried out in an argon atmosphere at heating and cooling rates of 10°C/min.

The phase composition of the alloys was determined by X-ray diffraction analysis on a D8 ADVANCE diffractometer (Bruker, United States) in CuK_α monochromatic radiation.

Brinell hardness was measured on a NEMESIS 9001 universal hardness tester (INNOVATEST, the Netherlands). The test parameters were as follows: a ball with a diameter of 2.5 mm, a load of 62.5 kgf (≈613 N), and holding time under load of 10 s.

The electrical conductivity of the bronzes was determined using a contact-free eddy current conductivity meter VE-27NC (NPP Sigma, Russia) with a measurement range of 5–37 MS/m. Further, to calculate the thermal conductivity (λ), we used the empirical relation connecting thermal conductivity with electrical conductivity, proposed by Smith and Palmer [26], which has the form

$$\lambda = AL_0T\sigma + B, \quad (2)$$

where L_0 is the Lorentz number, T is temperature, σ is electrical conductivity, and A and B are empirical constants (for copper alloys $A = 0.967$ and $B = 7.53$ W/(m K) [26]).

Mechanical properties were investigated on cylindrical specimens with a diameter of 5 mm and a length of the working part of 60 mm. Tensile tests were carried out on a 5569 universal testing machine (Instron, United States). Three samples were tested for each alloy and cooling rate.

Equilibrium and nonequilibrium solidification pathway curves were calculated using the ThermoCalc software [27] and the TCBIN thermodynamic base (Binary alloys database) [28].

Tribological studies were carried out according to the “shaft–partial insert” scheme using a T-05 tribometer (Institute for Sustainable Technologies, Poland). The insert specimen was a parallelepiped of the studied bronze with dimensions 15.75 × 10.00 × 6.35 mm, having a radius groove for a counter-body in the form of a ring with a diameter of 35 mm from steel (Fe–0.3C–3Cr–1W–0.45Mn–0.3Si). The surface of the counter-body was subjected to nitriding. Two samples were tested for each alloy and cooling rate. The

tests were carried out in a medium of TS-1 kerosene at room temperature, but during the tests it increased to 80–90°C. The sliding speed and load were $v = 2$ m/s and $N = 627$ N, respectively. The duration of the test was 1 h.

The linear wear rate (I_h) was calculated by the formula

$$I_h = h/L = h/(vt), \quad (3)$$

where h is linear wear, L is friction path, v is sliding speed and t is test time.

Linear wear (h , m) was calculated by the equation

$$h = \Delta m/(Sp), \quad (4)$$

where Δm is the change in mass that occurs after abrasion of the sample, S is the area of the working surface of the sample, and ρ is the density of the bronze.

The weights of the samples before and after the tests were measured on a Kern 770 balance with an accuracy of 1 mg. The surface area of the sample in contact with the counter-body was 1 cm² and the density of bronze samples, determined using hydrostatic weighing, was 8873 kg/m³.

After the wear test, an additional test was carried out immediately to evaluate the coefficient of friction. For this, the rotation drive was stopped and the readings of the friction force sensor were zeroed at a steady temperature. Then the drive was switched on again for 5 min and the friction force was recorded. The friction coefficient (μ) was calculated as the ratio of the steady-state friction force to the load $\mu = F_{tr}/N$.

RESULTS AND DISCUSSION

Figure 1 shows the cooling curves recorded when pouring ingots from C92900 bronze into sand, steel, and graphite molds. Since ingots were poured from alloys corresponding in composition to the lower (L) and upper (U) alloying limits, two curves were obtained for each mold material. The average values of the cooling rate (v_{cool}) in the range from the pouring temperature 1100 (pouring temperature) to 400°C. Its minimum value (0.4°C/s) was obtained by pouring bronze into a sand mold. When using steel and graphite molds, the cooling rate was 5.0 and 14.6°C/s, respectively; i.e., in comparison with casting into a sand mold, the values of v_{cool} increased 12.5 and 36.5 times. It should be borne in mind that the difference in cooling rates is provided not only by the difference in the thermophysical properties of materials, but also by the difference in the sizes of the ingots.

According to the results of differential scanning calorimetry (Fig. 2) for the alloy alloyed at the lower limit, the liquidus and solidus temperatures were 1002 and 829°C, respectively, and alloying the alloy at the upper limit leads to their decrease to 990 and 787°C, respectively.

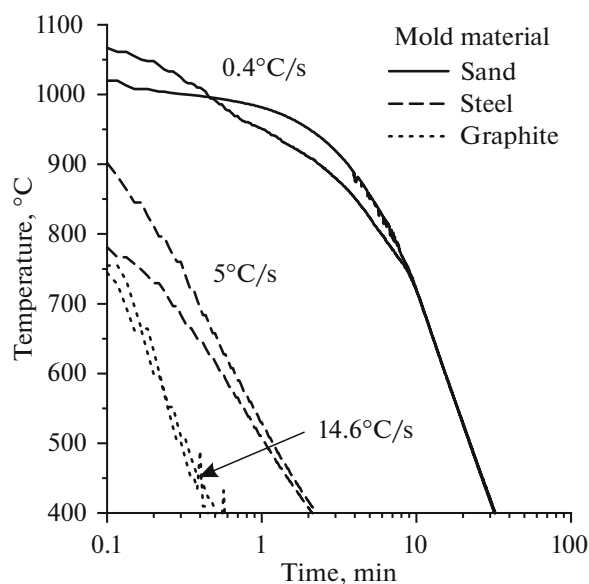


Fig. 1. Cooling curves recorded in the course of pouring C92900 ingots into sand, steel, and graphite molds. Numbers on the graph show the average cooling rate in the temperature range 1100–400°C.

Thus, a variation in the composition of C92900 bronze within the limits established by the UNS can lead to a change in the solidus temperature by 40°C, which must be taken into account in the case of subsequent deformation or heat treatment.

Figure 3 shows the macrostructure of alloys *L* and *U* when pouring into molds made of steel and graphite. It can be seen that varying the alloy composition within the limits specified in the standard for C92900 bronze does not lead to a change in the macrostructure. Only the cooling rate has an effect on the grain size in alloys.

The grain size of C92900 bronze (alloys *L* and *U*), depending on the cooling rate, is shown in Fig. 4. It can be seen that its increase from 0.4 to 5°C/s leads to a decrease in the grain size from 1920 to 229 μm for alloy *L* and from 1600 to 202 μm for alloy *U*; that is, the grain is refined 7–8 times. A further increase in the cooling rate, which is provided when casting in graphite mold, contributes to a decrease in grain size to 74 and 90 μm for alloys *L* and *U*, respectively. The influence of the alloy composition on the grain size in comparison with the cooling rate is not as significant.

Figure 5 shows the microstructure of C92900 bronze alloyed at the lower and upper limits when poured into sand, steel, and graphite molds. In addition to the copper-based solid solution indicated in the microstructure images as (Cu), the alloy structure contains the γ -Cu₃Sn intermetallic phase, lead-based solid solution (Pb), and copper-based solid solution (Cu)'—differing in composition from (Cu).

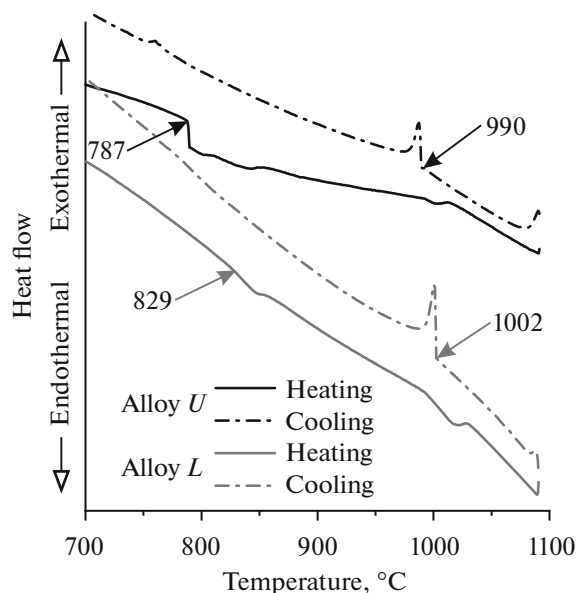


Fig. 2. DSC curves for C92900 bronze alloyed along the lower (alloy *L*) and upper (alloy *U*) limits

It is seen that, with an increase in the cooling rate, the size of the dendritic cells of the solid solution based on copper (Cu) and other phase components decreases and the (Pb) particles are spheroidized.

It is rather difficult to establish the difference in the tin content between the (Cu) and (Cu)' phases, since significant dendritic segregation is observed in the dendrites of the copper solid solution. Thus, the Sn content in the center and at the boundaries of the dendritic cells of alloys obtained in steel and graphite molds is ~2 and 8 at %, respectively. In the (Cu)' phase, the Sn concentration reaches 3.5–4.0 at %. A significant difference between the above phases can be established by the Ni content. Thus, (Cu) contains 3–4 at % Ni in alloy *L* and 4–5 at % Ni in alloy *U* and, in (Cu)', about 0.7 at % Ni.

Thus, the segregation of Ni is significantly less than that of Sn. It should also be noted that the cooling rate has practically no effect on the Ni content in the above phases.

In [1–3, 6, 7], based on the analysis of the binary Cu–Sn phase diagram [29], it is indicated that the Sn-rich intermetallic phase δ -Cu₃Sn₈ formed as a result of eutectoid transformation. At the same time, the authors of [30] studied the solidification process of the Cu–15 wt % Ni–8 wt % Sn alloy. Alloy samples were quenched from liquid and solid states at different temperatures. It was found that, upon quenching from 870–750°C, a solid solution based on copper (Cu) and the γ -(Cu,Ni)₃Sn phase with the DO₃ structure located along the boundaries of dendritic cells (divorced eutectic), were observed in the alloy structure. The formation of γ -(Cu,Ni)₃Sn phase from a liq-

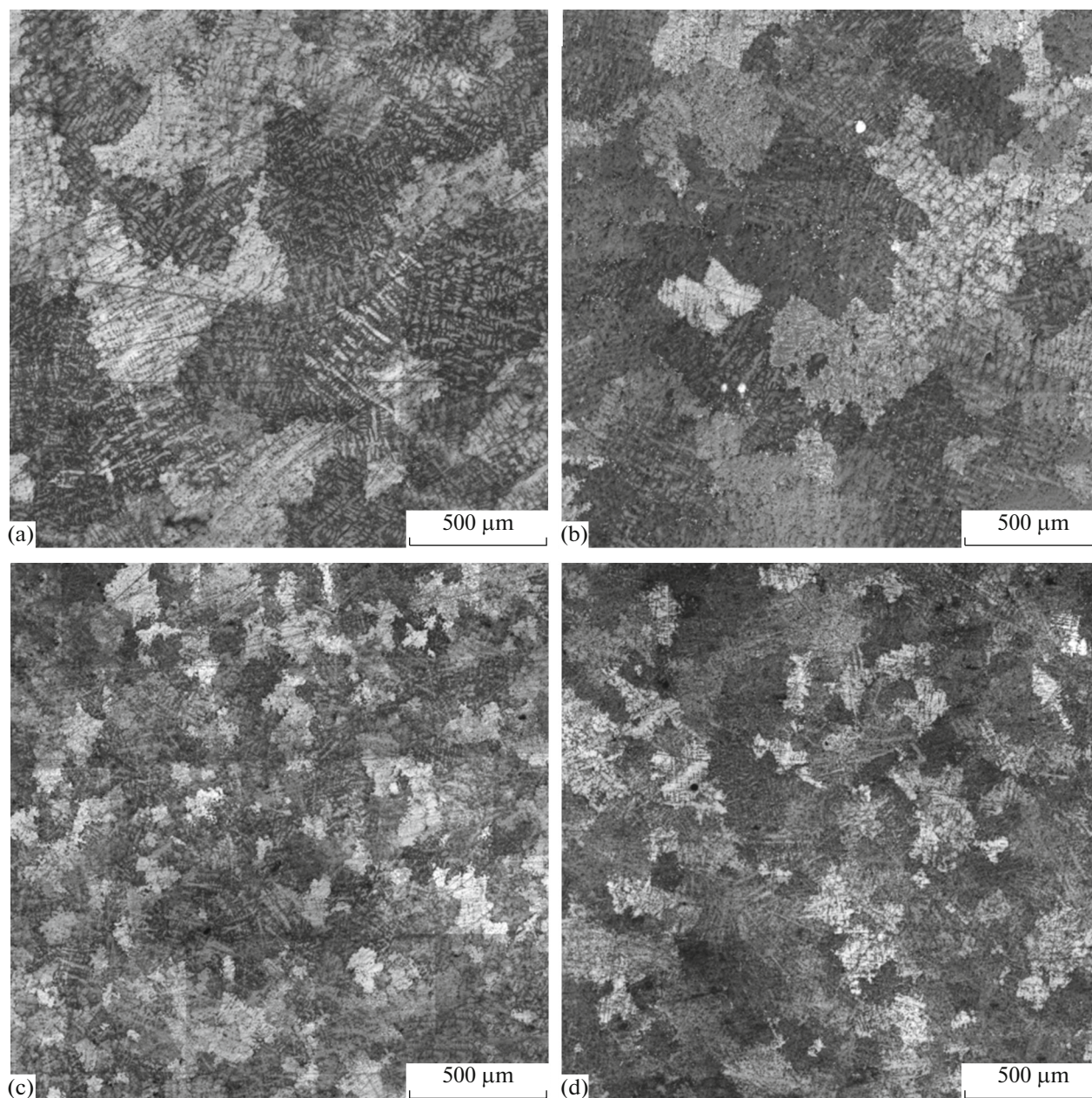


Fig. 3. Macrostructure of C92900 bronze cast into steel (a, b) and graphite (c, d) molds. (a, c) Alloying at the lower limit (alloy *L*); (b, d) at the upper limit (alloy *U*).

uid was also confirmed by thermodynamic calculations [31].

In [8], the authors found that, in addition to lead particles uniformly distributed in the matrix, there are lead particles that nucleated on particles and around particles of the Cu–Sn intermetallic phase located along the boundaries of dendritic cells, which also indicates the formation of an intermetallic phase by the eutectic transition.

Due to the absence of a thermodynamic database that includes all components of the C92900 bronze, the Thermo-Calc software package was used for cal-

culcation of the equilibrium and non-equilibrium (according to the Scheil–Gulliver model) solidification for binary Cu–Sn alloys containing 9 and 11 wt % Sn (Fig. 6). It is known that nickel is infinite soluble in both liquid and solid copper, which means that it will not form new phases. As for lead, it solidified as a individual phase (Pb) at the end of the solidification process. On this basis, it can be assumed that, for binary alloys Cu–Sn and C92900 bronze, the solidification pathway should be similar. With equilibrium solidification, only (Cu) crystals should form in the structure of both alloys, and with non-equilibrium, the appear-

ance of an intermetallic γ -Cu₃Sn phase is possible by eutectic reaction.

Thus, the most probable mechanism for the formation of an intermetallic phase during non-equilibrium solidification in the structure of tin bronzes is a eutectic rather than a eutectoid transformation.

The content of elements in the Cu₃Sn phase, determined by X-ray microanalysis, depending on the cooling rate for alloys *L* and *U*, is shown in Fig. 7. Since Cu and Ni are infinitely soluble in each other in both liquid and solid states [32], this phase is a ternary γ -(Cu,Ni)₃Sn, but for simplicity we denote it as binary (Cu₃Sn). It is seen that the content of Ni and Sn in it in alloys *L* and *U* when poured into a sand mold ($v_{\text{cool}} = 0.4^\circ\text{C/s}$) practically coincides (13–14 and 25 at %, respectively). At cooling rates of 5 and 14.6°C/s (casting into steel and graphite molds, respectively), the composition of the Cu₃Sn phase is almost the same for different mold materials, but different for alloys *L* and *U*: for alloy alloyed to the lower limit, Ni and Sn content in the Cu₃Sn phase are 7.5 and 22 at %, respectively and, for the alloy alloyed at the upper limit, 10 and 24 at %. Thus, an increase in the cooling rate leads to a decrease in the concentration of nickel in the Cu₃Sn phase.

Figure 8 shows the effect of the cooling rate on the volume fraction of phases in the structure of C92900 bronze (alloys *L* and *U*). It can be seen that it has the greatest effect on the content of the (Cu)' phase. Thus, for its small value ($v_{\text{cool}} = 0.4^\circ\text{C/s}$), realized when casting into sand molds, the fraction of this phase is maximum and, for alloys *L* and *U*, it is 4.7 and 7.5 vol %, respectively. An increase in the cooling rate to 5°C/s leads to a decrease in the fraction of the (Cu)' phase to 0.9 and 0.6 vol % for alloys *L* and *U*, respectively. This phase is absent in the structure of alloys obtained by casting into graphite molds ($v_{\text{cool}} = 14.6^\circ\text{C/s}$).

Usually, an increase in the cooling rate leads to an increase in the fraction of nonequilibrium phases in the structure of the alloy [33]. Apparently, in this case, the (Cu)' phase is formed not during the solidification of the alloy, but during its cooling in the solid state; an increase in the cooling rate does not allow the phase transformation along which the (Cu)' phase is formed to occur.

The volume fraction of a solid solution based on lead (Pb) practically does not change with an increase in the cooling rate; it also depends little on the lead content in the alloy and amounts to ~2 vol %. As for the Cu₃Sn, it can be seen that, in the alloy alloyed according to the lower limit, its content does not change and is ~4 vol %. In an alloy alloyed over the upper limit, with an increase in the v_{cool} , the Cu₃Sn phase fraction decreases and amounts to 9.0, 7.8, and 6.7 vol % at cooling rates of 0.4, 5.0, and 14.6°C/s, respectively.

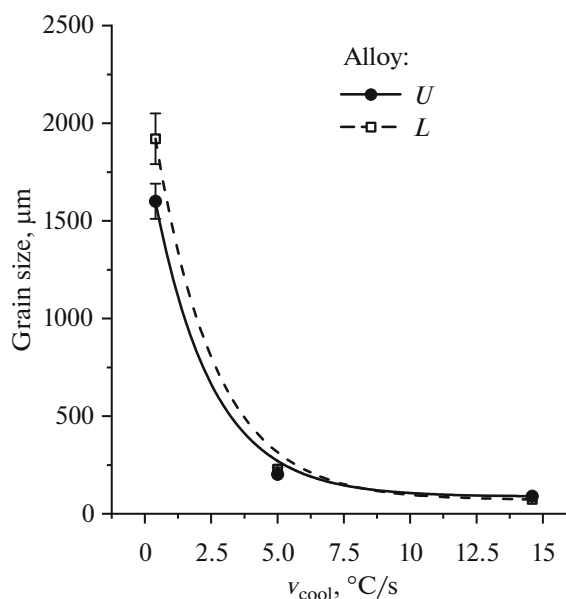


Fig. 4. Grain size of bronze ingots C92900 depending on the cooling rate.

According to [3], the fraction of the Cu₃Sn phase in the structure of C92900 bronze should be 4.5–9.0 vol %. The results show that, to fulfill this condition, it is sufficient to provide the content of alloying elements in the alloy closer to the upper alloying limit.

A change in the cooling rate has a weak effect on the Feret diameter and the circularity of the particles of the Cu₃Sn and (Cu)' phases, and therefore it is not considered. Fig. 9 shows the Feret diameter and the circularity of the (Pb) phase particles in C92900 bronze depending on the cooling rate for alloys alloyed at the lower and upper limits. It can be seen that both shape parameters practically do not differ for alloys *L* and *U*.

As for the (Pb) phase, the cooling rate significantly affects its particle shape. For $v_{\text{cool}} = 0.4, 5.0,$ and 14.6°C/s , the Feret diameter for the (Pb) phase is ~3.7, 2.8, and 2.4 μm, respectively; i.e., with an increase in the cooling rate, the size of lead particles in the alloy structure decreases. The circularity of particles (Pb) at $v_{\text{cool}} = 0.4, 5.0,$ and 14.6°C/s is 0.5, 0.6, and 0.7, respectively. It follows from this that, with an increase in the cooling rate, there is not only a decrease in the particle size, but also a change in their shape to a more spherical one.

The results of X-ray phase analysis for C92900 bronze, obtained in the sand, steel, and graphite molds and alloyed on the lower (*L*) and upper (*U*) limits are shown in Fig. 10. As can be seen, it was possible to identify only solid solutions based on copper (Cu) and lead (Pb). As for Cu₃Sn, then the only peak of it coincided with the (Cu) peak. In [20], the authors also experienced difficulties in identifying the intermetallic

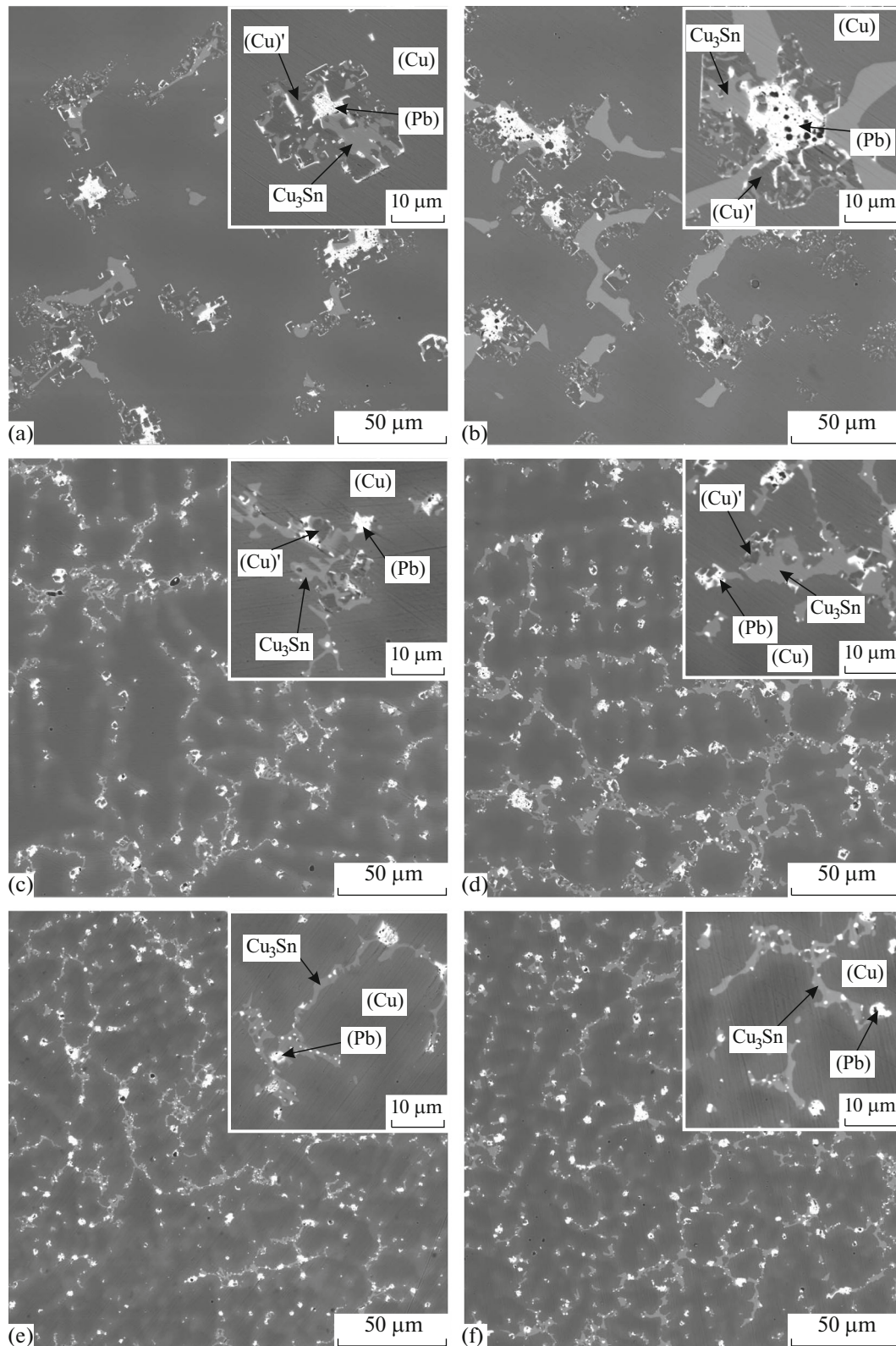


Fig. 5. Microstructure of C92900 bronze, poured into sand (a, b), steel (c, d), and graphite (e, f) molds. (a, c, e) Alloying at the lower limit (alloy *L*) and (b, d, f) the upper limit (alloy *U*).

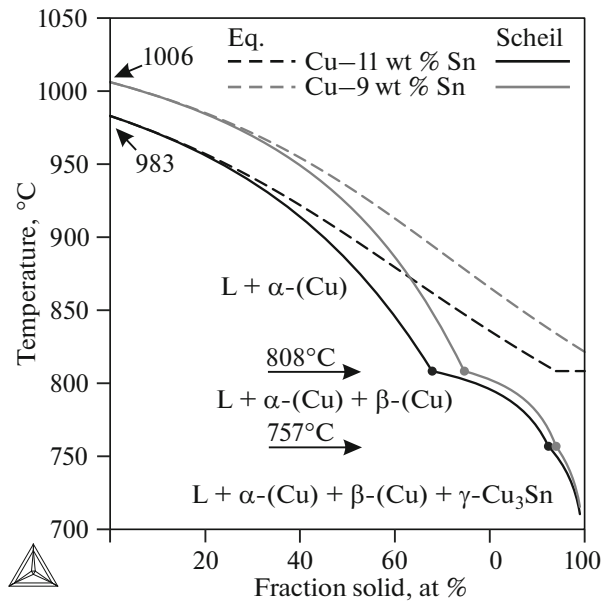


Fig. 6. Curves of equilibrium and nonequilibrium (according to the Scheil–Gulliver model) solidification pathway calculated in the Thermo-Calc software for binary alloys Cu–9 wt % Sn and Cu–11 wt % Sn.

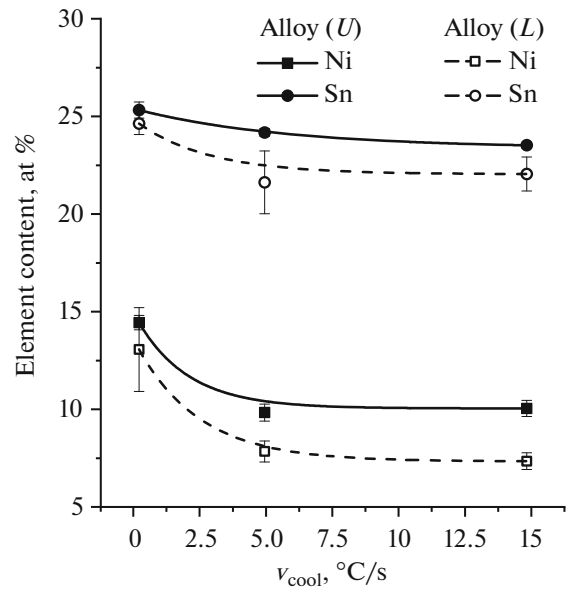


Fig. 7. Content of Ni and Sn in the Cu_3Sn phase in C92900 bronze, depending on the cooling rate.

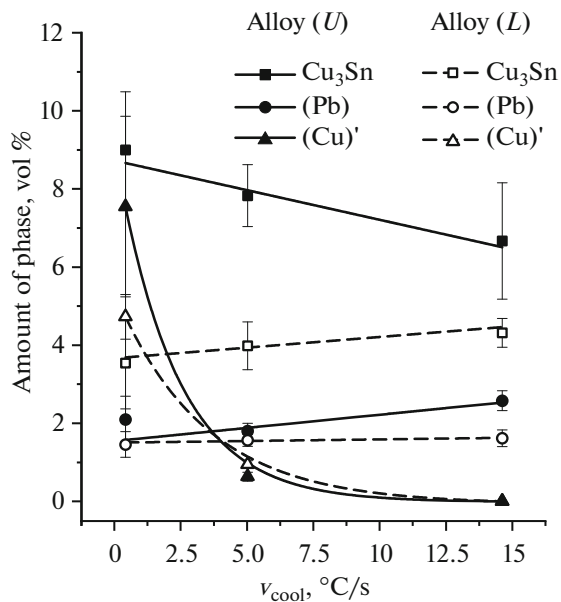


Fig. 8. Volume fraction of phases in C92900 bronze, depending on the cooling rate.

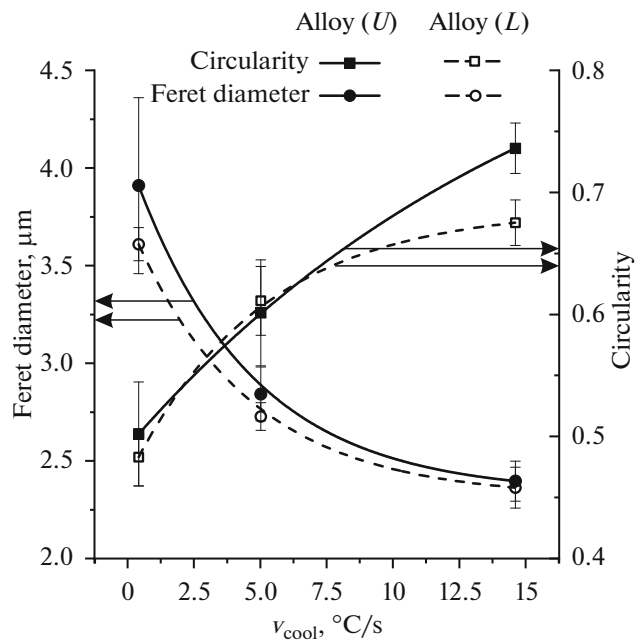


Fig. 9. Feret diameter and circularity of (Pb) phase particles in C92900 bronze, depending on the cooling rate.

phase in tin bronze. The (Cu)' phase could not be identified, since it differs from the (Cu) phase only in the Ni content and its peaks should practically coincide with (Cu). It can be seen that neither the cooling rate nor alloying along the upper and lower limits led to a change in the phase composition of the alloy.

It is known that the wear resistance of the material is influenced by the temperature regime of the part [34]. The higher the thermal conductivity (λ) is, the better the heat removal from the friction edge and the less oxidation of the friction materials. Also, when heated, the hardness of the antifriction layer decreases

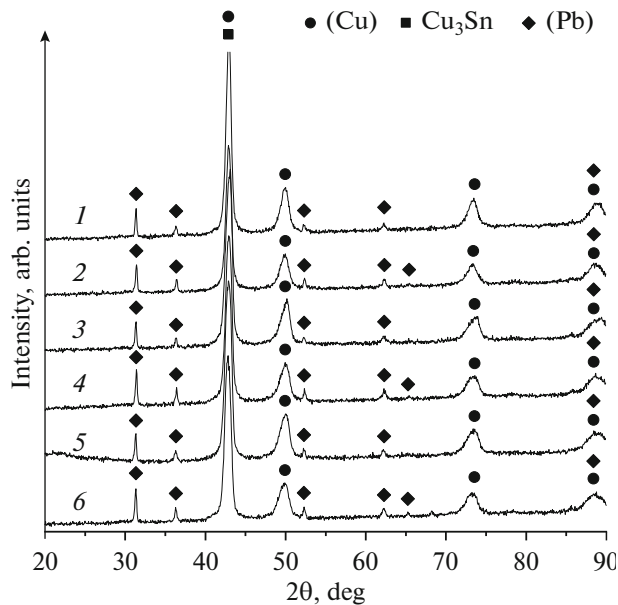


Fig. 10. Results of X-ray diffraction analysis of C92900 bronze samples poured into sand (1, 2), steel (3, 4), and graphite (5, 6) molds. (1, 3, 5) Alloying at the lower limit (alloy *L*) and (2, 4, 6) the upper limit (alloy *U*).

and the tendency to sticking and scuffing in friction pairs increases [35].

Figure 11 shows the thermal conductivity of C92900 bronze obtained in the sand, steel, and graphite molds, alloyed along the lower (*L*) and upper (*U*) limits, depending on the cooling rate. It can be seen

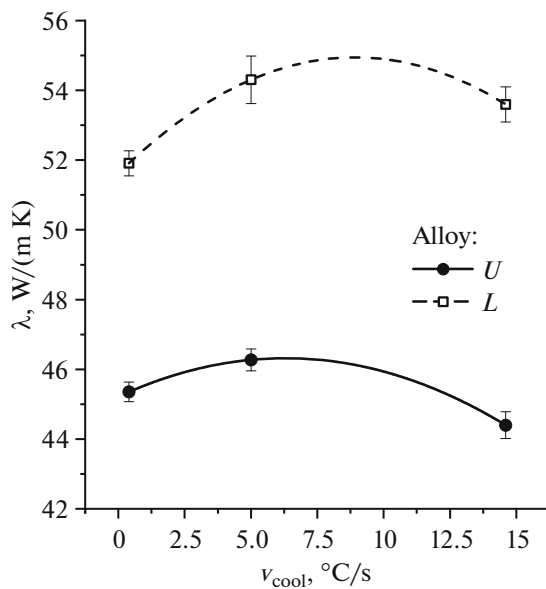


Fig. 11. Thermal conductivity of C92900 bronze as a function of the cooling rate.

that it practically does not change the thermal conductivity of the alloys. To a much greater extent, thermal conductivity is influenced by the content of alloying elements in bronze. Therefore, alloy *L* has a thermal conductivity of $\lambda = 52\text{--}54$ W/(m K), and the alloy *U* 44–46 W/(m K). According to the data of [36] for the Cu_3Sn at a temperature of 25°C, the value of λ is 72 W/(m K), i.e., exceeds the thermal conductivity of copper solid solution. On the other hand, it should be taken into account that, in the case under consideration, Cu_3Sn also contains nickel, which can lead to a decrease in λ values. Therefore, it is impossible to say unambiguously what exactly influences the thermal conductivity of the alloy to a greater extent, the content of Sn and Ni in (Cu) or the amount and distribution of the Cu_3Sn phase.

When an alloy is used for friction, one very important characteristic is its hardness. Figure 12 shows the dependence of the hardness of C92900 bronze on the cooling rate for alloys alloyed according to the lower (*L*) and upper (*U*) limits. It can be seen that, for alloy *L*, hardness at $v_{cool} = 0.4, 5.0$ and 14.6°C/s is 98, 116, and 121 HB, respectively, and, for alloy *U*, 103, 128, and 133 HB. Hence, it follows that the increase in hardness is facilitated by both an increase in the cooling rate and an increase in the content of alloying elements in the alloy. Note that a change in the cooling rate from 5 to 14.6°C/s has practically no effect on the hardness of the alloy.

Figure 13 shows the effect of the cooling rate on the mechanical properties of C92900 bronze alloyed with the lower (*L*) and upper (*U*) limits. It can be seen that,

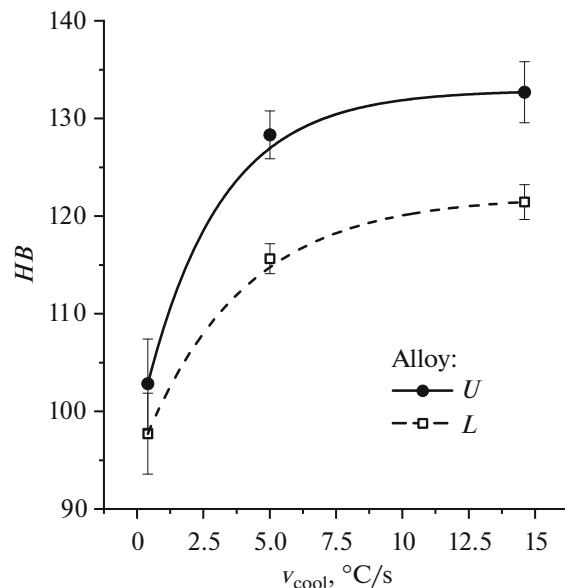


Fig. 12. Hardness of C92900 bronze as a function of the cooling rate.

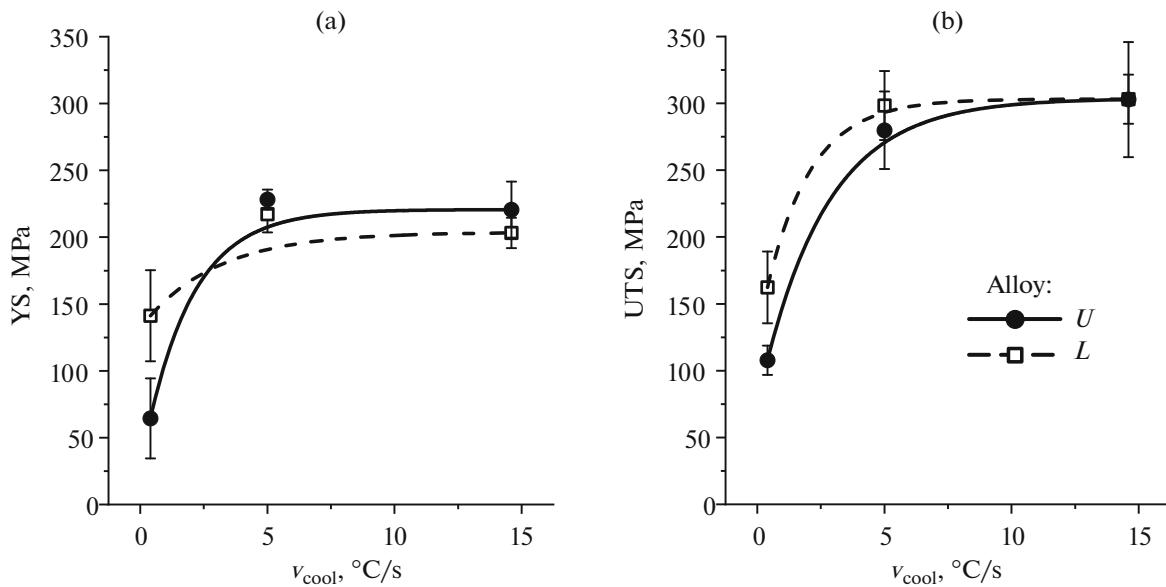


Fig. 13. YS (a) and UTS (b) of C92900 bronze, depending on the cooling rate during tensile tests.

taking into account the confidence interval, the content of alloying elements has practically no effect on the ultimate tensile strength (UTS) and yield strength (YS) of bronze. For $v_{cool} = 0.4, 5.0$ and 14.6°C/s , the YS = 103, 222, and 212 MPa, and the UTS = 135, 289, and 303 MPa.

Shrinkage porosity was clearly observed at the fractures of the samples, especially those obtained in sand molds, in the place of fracture. This explains the very low values of the YS and UTS (<150 MPa) and elongation at fracture ($EI = 1\text{--}5\%$), as well as significant confidence intervals when testing specimens poured into a sand mold.

In general, it can be concluded that an increase in the cooling rate leads to an increase in the strength of bronze and a change in the content of elements in bronze within the UNS does not significantly affect the mechanical properties.

Figure 14 shows the effect of the cooling rate on the wear rate and the coefficient of friction of C92900 bronze alloyed along the lower (L) and upper (U) limits. Despite the large values of the confidence intervals, it can be seen that an increase in the cooling rate from 0.4 to $5.0\text{--}14.6^{\circ}\text{C/s}$ leads to an increase in the wear rate from $\sim 0.4 \times 10^{-8}$ to $\sim 1.2 \times 10^{-8}$ and the coefficient of friction from ~ 0.04 to 0.06 . The chemical composition of bronze has practically no effect on the wear rate. The results indicate that the wear of C92900 bronze is largely influenced not by the fraction of Cu_3Sn and (Pb) phases, but their size and distribution in the alloy structure, which depend on the cooling rate.

Thus, obtaining ingots from C92900 bronze in steel and graphite molds provides higher mechanical properties, but at the same time leads to a slight decrease in wear resistance, which should be taken into account when choosing a casting method for ingots from this material.

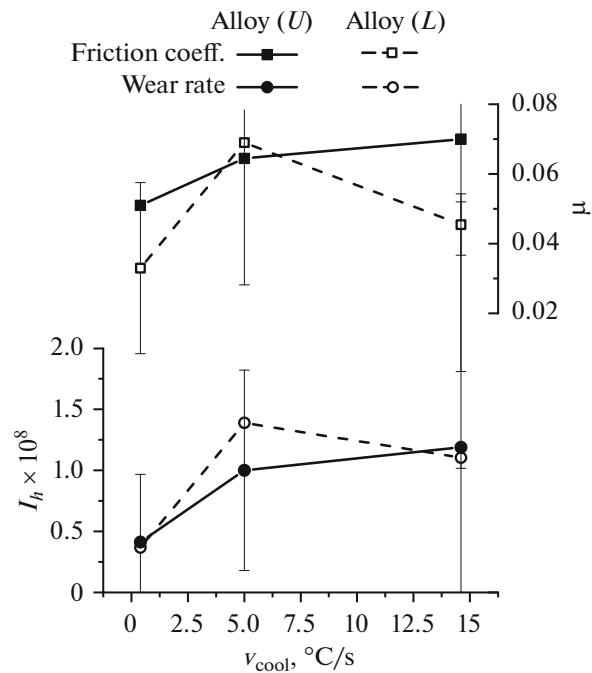


Fig. 14. Wear rate (I_h) and friction coefficient (μ) of C92900 bronze, depending on the cooling rate.

CONCLUSIONS

(1) Alloying C92900 bronze according to the upper limit established by UNS leads to a decrease in the solidus temperature by 40°C, which should be taken into account when assigning deformation and heat-treatment regimes.

(2) An increase in the cooling rate from 0.4 to 14.6°C/s during the solidification of ingots from C92900 bronze leads to a significant grain refinement from 1800 to 80 μm. At the same time, the change in the composition of bronze within the limits established by the UNS has practically no effect on the grain size.

(3) The cooling rate during solidification affects both the amount and the size and morphology of phases in the structure of C92900 bronze. As the cooling rate increases, the size decreases and the circularity of the lead particles increases. As for the γ -(Cu,Ni)₃Sn phase, its amount in the structure of bronze is then largely influenced by the content of tin, and its high fraction is observed when alloying along the upper limit of the content of alloying components in the alloy.

(4) The thermal conductivity of the studied bronze is practically independent of the cooling rate and is 45–55 W/(m K). As for the hardness, it increases both with an increase in the cooling rate and with alloying along the upper limit. Its minimum value was 100 HB, and its maximum value was 130 HB.

(5) An increase in the cooling rate leads to an increase in the strength of bronze, and the change in the content of alloying elements within the UNS does not significantly affect the mechanical properties. Thus, the ultimate strength with an increase in the cooling rate from 0.4 to 14.6°C/s increased from 150 to 300 MPa.

(6) The change in the composition of C92900 bronze within the UNS practically does not affect the wear rate. As for the effect of the cooling rate, its increase leads to an increase in the wear rate of bronze samples.

FUNDING

This research received financial support from the Ministry of Science and Higher Education in the Russian Federation (Agreement No. 075-11-2019-045 from November 22, 2019) under the program “Scientific and Technological Development of the Russian Federation” as per governmental decree no. 218 dated April 9, 2010.

CONFLICT OF INTEREST

The authors declare that they have no conflict of interest.

REFERENCES

- Gruzdeva, I.A., Sulitsyn, A.V., Mysik, R.K., and Sokunov, B.A., The effect of electromagnetic stirring on the structure and properties of tin bronzes, *Liteishchik Ross.*, 2006, no. 11, pp. 27–29.
- Song, K., Zhou, Y., Zhao, P., Zhang, Y., and Bai, N., Cu–10Sn–4Ni–3Pb alloy prepared by crystallization under pressure: An experimental study, *Acta Metall. Sin.*, 2013, vol. 26, pp. 199–205.
- Belov, V.D., Gerasimenko, E.A., Guseva, V.V., and Konovalov, A.N., Influence of solidification conditions of tin bronze C92900 parts on its structure, *Liteinoe Proizvod.*, 2016, no. 2, pp. 26–33.
- Ozerdem, M.S. and Kolukisa, S., Artificial neural network approach to predict the mechanical properties of Cu–Sn–Pb–Zn–Ni cast alloys, *Mater. Des.*, 2009, vol. 30, pp. 764–769.
- Brontvain, L.R., Investigation of the mechanical properties of bronze depending on the casting method, *Liteinoe Proizvod.*, 1966, no. 12, p. 31.
- Nyysönen, T., Leaded tin bronzes: the effects of casting method on dry sliding behavior, *Tribologia*, 2012, vol. 31, pp. 4–11.
- Chen, X., Wang, Z., Ding, D., Tang, H., Qiu, L., Luo, X., and Shi, G., Strengthening and toughening strategies for tin bronze alloy through fabricating in-situ nanostructured grains, *Mater. Des.*, 2015, vol. 66, pp. 60–66.
- Prasad, B.K., Patwardhan, A.K., and Yegneswaran, A.H., Factors controlling dry sliding wear behaviour of a leaded tin bronze, *Mater. Sci. Technol.*, 1996, vol. 12, pp. 427–435.
- Prasad, B.K., Sliding wear behaviour of bronzes under varying material composition, microstructure and test conditions, *Wear*, 2004, vol. 257, pp. 110–123.
- Equey, S., Houriet, A., and Mischler, S., Wear and frictional mechanisms of copper-based bearing alloys, *Wear*, 2011, vol. 273, pp. 9–16.
- Aksoy, M., Kuzucu, V., and Turhan, H., A note on the effect of phosphorus on the microstructure and mechanical properties of leaded-tin bronze, *J. Mater. Process. Technol.*, 2002, vol. 124, pp. 113–119.
- Belousov, A.A., Pastukhov, E.A., and Chentsov, V.P., Influence of dissolved nickel and temperature on the oxidation kinetics of lead tin free bronzes, *Rasplavy*, 2005, no. 2, pp. 8–10.
- Ryzhikov, A.A., Timofeev, G.I., and Lebedev, P.V., Features of tin bronze castings solidification, *Liteinoe Proizvod.*, 1968, no. 9, pp. 23–25.
- Vershinin, P.I., Sevast'yanov, V.I., and Bakrin, Yu.N., Effect of cooling intensification on the structure and properties of tin bronze castings, *Liteinoe Proizvod.*, 1986, no. 5, pp. 8–9.
- Semenov, K.G., Koloskov, V.F., and Chursin, V.M., Development of the production technology of high-quality castings from tin bronze ingots, *Liteinoe Proizvod.*, 1994, no. 7, pp. 10–12.
- Brontvain, L.R. and Gorodetskii, V.N., Soundness of casting copper alloys, *Liteinoe Proizvod.*, 1985, no. 10, pp. 14–16.
- Fetisov, N.M., Ryumshin, N.A., Suponitskii, V.M., Litovchenko, V.I., Repina, N.I., Rudnitskaya, V.L., and Belozherov, V.F., Influence of mold heat capacity on the structure and properties of BrOCS 4-4-17 bronze castings, *Liteinoe Proizvod.*, 1973, no. 9, pp. 24–26.

18. Ruusila, V., Nyyssonen, T., Kallio, M., Vuorinen, P., Lehtovaara, A., Valtonen, K., and Kuokkala, V.-T., The effect of microstructure and lead content on the tribological properties of bearing alloys, *Proc. Inst. Mech. Eng., Part J*, 2013, vol. 227, pp. 878–887.
19. Brontvain, L.R. and Gorovetskii, V.N., Study of wear resistance of copper-based alloys, *Liteinoe Proizvod.*, 1981, no. 10, pp. 8–9.
20. Martyshev, N.V., Plotnikova, N.V., Skiba, V.Yu., Popelyukh, A.I., and Semenov, I.V., Influence of the BrOS10-10 bronze cooling rate on the structure, phase composition and cyclic durability of castings, *Obrab. Met.*, 2012, no. 3, pp. 67–70.
21. Martyshev, N.V. and Semenov, I.V., Structure and properties of bronze castings under different cooling rates, *Sovrem. Probl. Nauki Obraz.*, 2012, no. 6, pp. 1–6.
22. Martyshev, N., Semenov, I.V., and Petrenko, Y.N., Structure and properties of leaded tin bronze under different crystallization conditions, *Adv. Mater. Res.*, 2013, vol. 872, pp. 89–93.
23. Martyshev, N.V., Influence of the low-melting phase inclusions morphology on the tribotechnical properties of bronzes, *Privolzh. Nauchn. Vestn.*, 2011, no. 2, pp. 8–11.
24. Yan, P., Wang, D., Yan, B., and Mo, F., Effect of size refinement and distribution of the lubricating lead phases in the spray forming high-lead tin bronze on wear rates, *Mod. Phys. Lett. B*, 2013, vol. 27, p. 1341019.
25. Image Processing and Analysis in Java. <https://imagej.nih.gov/ij/docs/menus/analyze.html>. Accessed February 19, 2020.
26. Zheng, X., Cahill, D., Krasnochtchekov, P., Averback, R., and Zhao, J., High-throughput thermal conductivity measurements of nickel solid solutions and the applicability of the Wiedemann-Franz law, *Acta Mater.*, 2007, vol. 55, pp. 5177–5185.
27. Andersson, J.O., Helander, T., Höglund, L., Shi, P.F., and Sundman, B., Thermo-Calc and DICTRA, Computational tools for materials science, *CALPHAD: Comput. Coupling Phase Diagrams Thermochem.*, 2002, vol. 26, pp. 273–312.
28. Thermo-Calc Software TCBDIN Binary Alloys Database. Accessed January 1, 2020.
29. Park, J.S., Park, C.W., and Lee, K.J., Implication of peritectic composition in historical high-tin bronze metallurgy, *Mater. Charact.*, 2009, vol. 60, pp. 1268–1275.
30. Guo, Z., Jie, J., Liu, S., Liu, J., Yue, S., Zhang, Y., and Li, T., Solidification characteristics and segregation behavior of Cu–15Ni–8Sn alloy, *Metall. Mater. Trans. A*, 2020, vol. 51, pp. 1229–1241.
31. Turhan, H., Aksoy, M., Kuzucu, V., and Yildirim, M.M., The effect of manganese on the microstructure and mechanical properties of leaded-tin bronze, *J. Mater. Process. Technol.*, 2001, vol. 114, pp. 207–211.
32. Mey, S., Thermodynamic re-evaluation of the Cu–Ni system, *CALPHAD: Comput. Coupling Phase Diagrams Thermochem.*, 1992, vol. 16, pp. 255–260.
33. Scheil, E., Bemerkungen zur Schichtkristallbildung, *Z. Metallkd.*, 1942, vol. 34, pp. 70–72.
34. Alpas, A.T. and Zhang, J., Effect of microstructure (particulate size and volume fraction) and counterface material on the sliding wear resistance of particulate-reinforced aluminum matrix composites, *Metall. Mater. Trans. A*, 1994, vol. 25, pp. 969–983.
35. Andrusenko, O.E. and Matveev, Yu.I., Requirement for the materials of the anti-friction layer used in the restoration of plain bearings of crankshafts, *Vestn. Astrakh. Gos. Tekh. Univ. Ser.: Morsk. Tekh. Tekhnol.*, 2009, no. 1, pp. 50–55.
36. Kulikova, T.V., Bykov, V.A., Shunyaev, K.Yu., Yagodin, D.A., Petrova, S.A., and Zakharov, R.G., Investigation of the thermodynamic and thermophysical properties of the Cu₃Sn intermetallic compound, *Butlerov. Soobshch.*, 2011, vol. 27, no. 16, pp. 72–78.